Owen M. Williams, Nigel A. Spooner, Barnarby W. Smith, Jillian E. Moffatt
Extended duration optically stimulated luminescence in quartz
Radiation Measurements, 2018; 119:42-51

Final publication at http://dx.doi.org/10.1016/j.radmeas.2018.09.005

Extended Duration Optically Stimulated Luminescence in Quartz

Owen M. Williams[1], Nigel A. Spooner[1,2], Barnaby W. Smith[2] and Jillian E. Moffatt[1]

Abstract

As part of an investigation into the mechanisms underlying optically stimulated luminescence (OSL) in quartz, we have shone a number of South Australian natural quartzes over a six day measurement period. During this time the OSL signal was recorded over ten decades in time and fell six to seven decades in luminescent intensity. In particular, we observe the presence of a number of steps that appear when the luminescence is displayed in log/log form. In exploring the underlying mechanism, we review both the standard energy band gap model for quartz OSL and the alternative defect pair model and find that the latter can be applied to explain the steps in terms of a nearest neighbour extension.

1. Institute of Photonics and Advanced Sensing, School of Physical Sciences, University of Adelaide, Adelaide, Australia 5005

2. Weapons and Combat Systems Division, Defence Science and Technology Group, P.O. Box 1500, Edinburgh, Australia 5111

1. Introduction

The recent developments in automated luminescence readers have provided an opportunity that allows the mechanisms underlying optically stimulated luminescence (OSL) in quartz to be explored. For this purpose and as part of a wider study, we have used a combination of linearly modulated OSL (LM-OSL) and continuous wave OSL (CW-OSL) to shine a number of South Australian natural quartzes over a six day period. During this period we recorded the luminescent decay over almost ten decades in time and observed that the reduction in intensity covered six to seven decades.

Early studies directed towards elucidating the mechanisms underlying quartz thermoluminescence led to the development of the energy band gap model. [Refer, for example, to Aitken, 1985.] This has since become established as the standard in the field. Within the model, it is suggested that trapped electrons are excited into the conduction band. Luminescence is then emitted following subsequent radiative recombination with a hole trapped near to the valence band.

The energy band gap model was later adapted to describe OSL. In particular, the characteristic shape of the quartz OSL decay curves was first studied by Smith et al. (1986). More detailed observations were later reported by Smith and Rhodes (1994) who fitted the decay to a summation of three exponential components, commonly termed 'fast', 'medium' and 'slow'. Later, further slow components (Bulur et al., 2000, Singarayer and Bailey, 2003, Jain et al., 2003) and an ultrafast component (Jain et al., 2008) were identified.

Bailey et al. (1997) adapted the three component model of Smith and Rhodes (1994) into an empirical band gap model, within which kinetic parameters were assigned to each component based on observations of the OSL emission. In a subsequent development, Bailey (2001) refined the model into the form that has since been used as the basis for most quartz OSL modelling. [Refer, for example, to Preusser et al., 2009.] Evidently, it is possible to construct empirical band gap models to explain many OSL decay features.

Our present study reveals even more complexity, in that we found that when we plotted each extended shine in log/log form, the luminescent decay appeared to cascade over a number of steps. The first step lasts for the order of a second, the second for thousands of seconds and the third for significantly longer. Although steps have been observed previously [see, for example, Ankjaergaard and Jain (2010) and Wallinga et al. (2008)], they have not been physically explained. Potentially, the band gap model could be extended by adding more components, but only at the expense of further increasing its complexity. Moreover, each additional component (of which many are required to replicate our present observations) needs to be linked to a separate physical process.

The physically-based defect pair model introduced by Itoh *et al.* (2001, 2002) does not have the same problems and therefore provides a useful alternative. In this model, both the OSL signal and the 110^{o}C and 325^{o}C thermoluminescence bands in quartz are readily explained in terms of the movement of charge carriers between defect sites. The thermoluminescence explanation has recently been extended by Williams and Spooner (2018) who showed that a common defect pair is responsible for emission in the 110^{o}C , 160°C and 220°C bands.

We believe that the defect pair model is capable of explaining many of the characteristics displayed by quartz OSL. To this end, in this paper we propose a relatively simple nearest neighbour extension that we show can be applied to explain the presence of the luminescent steps.

In Section 2 we describe our samples and in Section 3 our OSL measurement and data processing procedures. Details are relegated to the appendices. In Section 4 we present our OSL data and discuss our specific observations. Finally, in Section 5 we critique both the energy band gap and defect pair models and apply the latter to explain the steps.

2. Samples

Eight readily available quartz samples were tested within the present study: six from the stranded dune sequence in South-East South Australia (SESA), one from Baldina Creek in the mid-north of South Australia and a bleached sample comprised of sunlit surface sand collected at Long Beach near to Robe on the SESA coast. The latter provided a zero in age. The SESA dunes have been dated by a number of independent methods and the accumulated results have been assembled by Moffatt (2014). The data are replicated in Table 1.

Sample	Range/place of collection	Dose rate (Gy/ka)	D_e (Gy)	Age (ka)	Source
LB	Long Beach	0.64 ± 0.04	0	0	Moffatt (2014)
RB	Robe	0.5 (assumed)	0.4 ± 0.3	0.8 ± 0.6	Huntley et al. (1993b) – quartz inclusions
WK	Woakwine	0.54 ± 0.04	65 ± 2	120 ± 9	Banerjee et al. (2003)
		0.58 ± 0.01	69 ± 2	118 ± 4	Huntley et al. (1994)
		0.56 ± 0.01	73 ± 3	132 ± 6	Huntley et al. (1993a)
		0.56 ± 0.03	64 ± 6	114 ± 16	Huntley et al. (1993b) – quartz inclusions
		0.40 ± 0.02	47 ± 7	116 ± 16	Huntley et al. (1993b) – quartz inclusions
				120	Belperio and Cann (1990)
				120	Schwebel (1983)
ED	East Dairy	0.44 ± 0.01	128 ± 16	292 ± 25	Huntley and Prescott (2001)
				309	Schwebel (1983)
				200	Belperio and Cann (1990)
BA	Baker	0.47 ± 0.01	209 ± 16	456 ± 37	Huntley et al. (1993a)
		0.48 ± 0.02	187 ± 16	390 ± 40	Huntley et al. (1993b) – quartz inclusions
				500	Belperio and Cann (1990)
HA	Harper	0.48 ± 0.01	282 ± 20	585 ± 44	Huntley et al. (1993a)
				650	Belperio and Cann (1990)
NE	Naracoorte East	0.63 ± 0.02	455 ± 44	720 ± 70	Huntley et al. (1993a)
				>860	Belperio and Cann (1990)
				950	Huntley *et el*. (1994) – oxygen isotope
				>780	Huntley *et el*. (1994) – magnetic reversal
BD	Baldina Creek	3.29 ± 0.08	262 ± 68	80 ± 21	Moffatt (2014)
				60 ± 6	Grün et al. (2008) – ESR on teeth

Table 1: South Australia quartz dating data

All samples were exposed to red light only during their recovery, transport, handling and preparation. The following laboratory processing steps were applied. Calcium carbonate was removed by reaction with HCl, while in a second step fine clay was removed by suspension, following dispersion in an NaOH ultrasonic bath. Feldspars and heavy grains were then density-separated and the remaining quartz grains were etched in 40% HF for forty minutes in order to remove any residual feldspar and to remove the outer 6-8 µm layer. The grains were rinsed in HCl to remove any fluoride components that may have been deposited during the etching process and were finally rinsed in distilled water before drying and sieving into size ranges. More precise processing details are given by Moffatt (2014).

The grain size range 125-180 µm was chosen for the present study. Grain samples were loaded onto stainless steel discs previously sprayed with silicone oil through a 7 mm diameter mask. The samples were not mass-normalised.

3. Procedures

3.1 Measurement procedures

Each sample was subjected to the same set of measurements within a Risø DA-20 automated reader. [Bøtter-Jensen et al., 2000, 2003; Risø, 2013.] In the present measurement series, band luminescence passed by a 7 mm thick Hoya U340 filter was recorded by the in-built EMI 9235QB photomultiplier tube (PMT). The filter passes ultraviolet radiation in a 300-390 nm band centred about 340 nm.

As stated above, the present program is directed towards gaining an improved understanding of the mechanisms underlying OSL in quartz. Sample variability is not addressed. Given the limited nature of our objective combined with the prolonged measurement period, only a single aliquot of each quartz was subjected to the six day shine procedure.

During each measurement period, the following steps were applied:

- TL to 260ºC at 5ºC/s was recorded.
- A 260ºC preheat was applied for 60 s in order to remove the thermally unstable OSL contributions.
- The disc was heated to 125ºC and the temperature allowed to settle for 30 s in order to offset thermal lag effects. The blue LEDs were then driven by a 10,000 s ramp towards 100% drive, during which time LM-OSL was recorded at 1 s bin sizes.
- The disc was again heated to 125ºC and temperature-settled before CW-OSL at 100% drive level was recorded over a 100,000 s period at 50 s bin sizes.
- The above step was repeated four times to complete ~500,000 s of combined LM-OSL and CW-OSL shine.

In separate calibration experiments we found that LM-OSL operation commenced after a small delay and slightly deviated from true linearity. These deviations from a perfect ramp were offset by applying the linearization transform described in Appendix A below. Each LM-OSL data set was smoothed by application of a custom algorithm, described in Appendix B.

Similar calibration experiments were conducted to examine the linearity of the subsequent CW-OSL sequences. In this case, no correction was required. The turn-on response time was always exceeded, even at the 1 ms minimum bin size. Hence, the optical output increased proportionately to the commanded drive level. The CW-OSL data were again smoothed by application of the custom algorithm.

3.2 Data gathering procedures

A typical LM-OSL signal is shown in Fig. 1(a). Two distinct peaks are clearly visible, as has been observed in previous studies. [See for example, Bulur et al., 2000, Kuhns et al., 2000, Oniya et al., 2012.] It is also noticeable that the luminescent decay appears to slow towards the end of the 10,000 s measurement period. The luminescence there, however, is by no means complete. We highlight also the presence of a small upward curvature following the post-threshold start, as can be seen in the expanded view shown in Fig. 1(b).

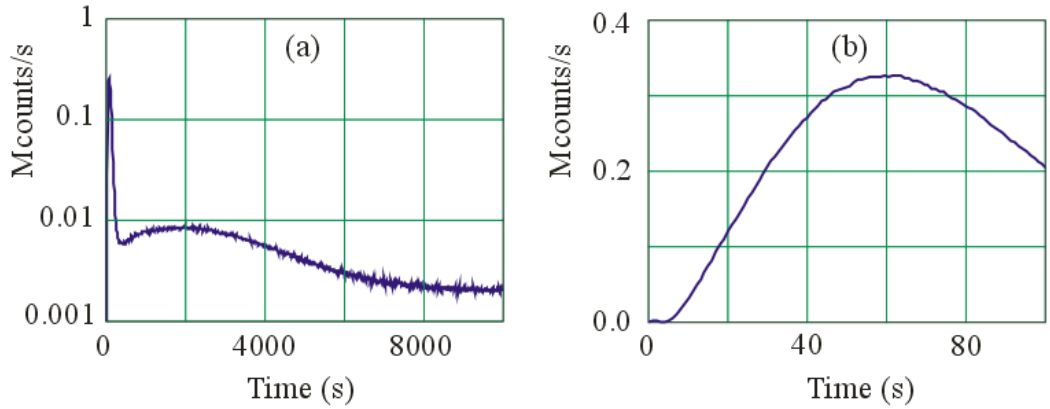

Fig. 1: Example of an unsmoothed Baker quartz LM-OSL response to a 100% drive ramp at 125ºC; (a) Entire shine; (b) Expanded view at small times

Our initial application of LM-OSL confers a number of advantages. Firstly, the saturation and pile-up effects that characterise bright SESA quartz samples are avoided due to the slow build-up of optical power. Secondly, as seen in Fig. 1, two luminescent components can readily be separated, while thirdly and perhaps most importantly, after the LM-OSL has been converted into an equivalent CW-OSL form (refer to Appendix C) we find that the luminescence at small shine times can be displayed at incredibly small bin widths.

In this respect, as we show below in Fig. 2, we gain the advantage that the shines can be extended over many decades in time without compromising the initial time resolution. By comparison, in the case of CW-OSL, the 10,000 bin limit imposed by the current Risø DA-20 operational software restricts the temporal dynamic range to four decades. At the highest resolution, the 1 ms bin time then limits the shine duration to 10 s.

A further restriction in the case of the bright quartzes studied here is that the LED drive level cannot exceed 5% of maximum if saturation effects are to be avoided. The effective 100% shine time therefore falls to 0.5 s. Another problem is then revealed; namely, we found that when we changed the OSL drive level between runs a discontinuity in recorded OSL level always occurred. Successive OSL runs could not therefore be properly merged. The same type of discontinuity also is seen in the earlier time-resolved OSL data reported by Ankjaergaard and Jain (2010).

Although we did not explore this effect in detail, its origin may be similar to the recuperation effect reported earlier by Aitken and Smith (1988). Instead, we overcame the problem experimentally. We found that no discernible discontinuity occurred when each new drive level was set the same as at the end of the preceding run. Our preference, then, has been to apply an initial LM-OSL run ramping towards 100% drive level and to later convert the data offline into an equivalent CW-OSL form (Appendix C). The initial run is then followed by a series of CW-OSL runs at 100% LED drive, during which time both the temporal and luminescence dynamic ranges are further extended.

4. Merged CW-OSL data

4.1 Merged data features

After application of the Appendix B smoothing procedures, we applied the general transform described below in Appendix C to convert the LM-OSL data into an equivalent CW-OSL form. This was then merged with the subsequent CW-OSL responses. An example of the merged response is shown in Fig. 2. The colours represent the successive LM-OSL and CW-OSL sequences while the dashed vertical lines indicate the merge times. The background has not been subtracted.

The original unsmoothed data are shown here in both linear/log and log/log forms. The absence of discontinuities between successive runs is clearly evident. Note that in view of the large dynamic ranges that have been achieved in both the time and luminescence domains, viewing the data in log/log form is our preferred option. We note further that the initial use of LM-OSL has allowed an equivalent CW-OSL rate in excess of 100 Mcounts/s to be recorded without saturation, and that data are available from incredibly early times.

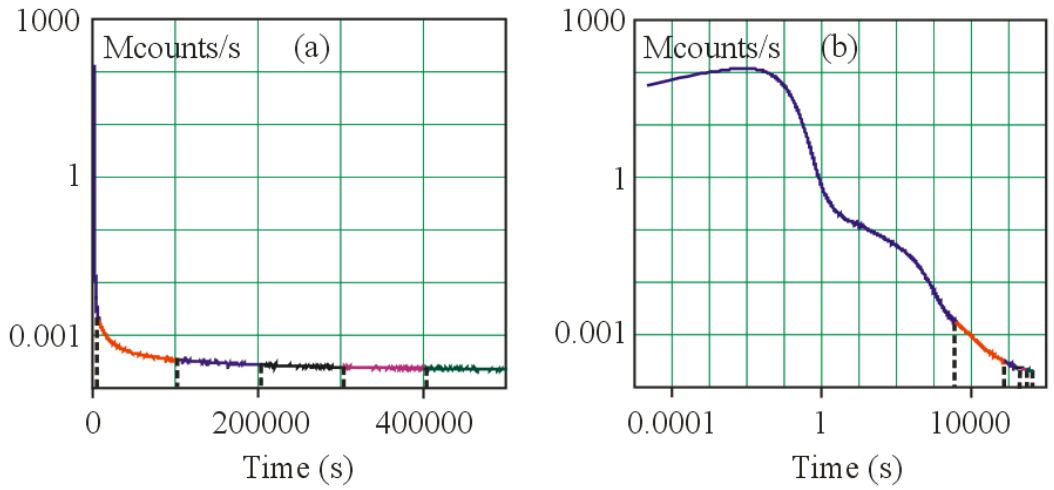

Fig. 2: (a) Linear/log and (b) log/log forms of the merged OSL response at 125ºC (Baker quartz). The dashed vertical lines represent the merge points.

A number of features are apparent. Firstly, the early response is so fast it cannot be resolved within the linear/log plot. In contrast, underlying structure is clearly observable within the log/log plot where interesting detail in the form of several luminescence steps is evident. The first two are readily apparent while a third is present but somewhat masked by the unsubtracted background.

Secondly, the shine signal is seen to persist for more than ten decades in time, during which period it falls across almost six decades in luminescence. Consistent with the square-law form of eqn (6) within Appendix C below, the bin widths at the start of the shine are remarkably small. Indeed, the concomitant increase in time resolution has allowed the early shine behaviour to be revealed. In particular, it is seen that the luminescence actually increases for a short time before trending downwards. This effect is consistent with the initial upward curvature seen within the Fig. 1(b) early LM-OSL response.

Thirdly and finally, we note that even towards the end of the six day measurement period, the shine is still incomplete. The luminescence signal is therefore remarkably persistent.

4.2 Log/log shine data display

The overall shine data are displayed in log/log form in Fig. 3. The labels correspond to (in order of increasing age): Long Beach (LB), Robe (RB), Baldina Creek (BD), Woakwine (WK), East Dairy (ED), Baker (BA), Harper (HA) and Naracoorte East (NE). The data have not been mass-normalised but the background has been subtracted. [Refer to Appendix A.2.] In the interests of clarity, the responses have been artificially separated by multiplying the measured count rates by the factors listed in the figure. The measured count rates can thus be simply restored. Note that we have included the cumulative stimulation energy within Fig. 3, calculated simply by multiplying the time values by the 40 mW/cm^2 of optical power delivered to each sample.

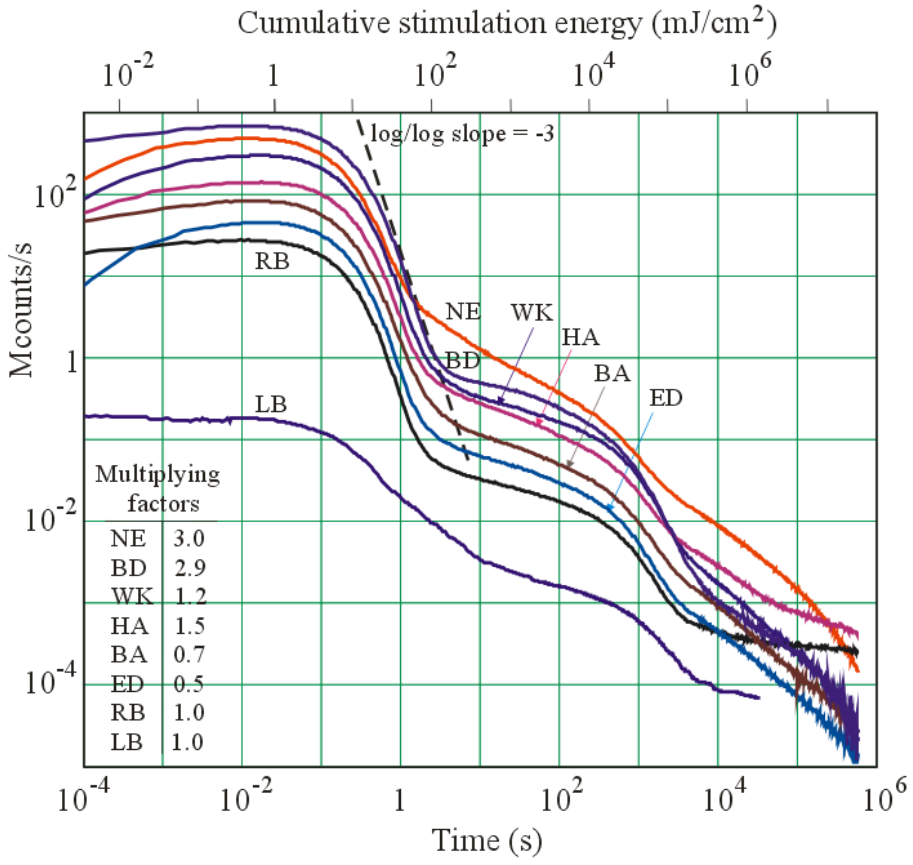

Fig. 3: Background-subtracted merged CW-OSL extended shine data at 125ºC

4.3 Observations

Within the present study, only a single aliquot of each quartz was shone. Given this limitation, it is only possible to comment qualitatively on the luminescent decay features seen in Fig. 3. Within the following subsections, we briefly discuss the most prominent of these; namely, the initial increase, the pronounced steps and the power law trends.

A number of other features clearly deserve attention. These form part of our wider research program. For example, the younger samples tend to be characterised by relatively sharp luminescence steps whereas in the case of the older samples, exemplified particularly by Naracoorte East (NE), the luminescent decay is more diffuse. We note further that the Long Beach (LB) sunlit sand sample still displays measureable luminescence (albeit two to three orders of magnitude smaller than the other samples). It appears therefore that strong sunlight is not capable of completely bleaching natural luminescence. It is also seen in this case that the second step is relatively stronger than in the case of each of the buried counterparts. The above observations and other details seen in Fig. 3, however, require further research consideration. As such, therefore, they lie outside of the scope of the present study.

4.3.1 Initial increase

Within Fig. 3 it is apparent that the luminescence increases initially, common to all shines except those for the youngest samples, LB and RB. For comparison purposes we conducted a separate CW-OSL experiment, selecting a Naracoorte East (NE) sample for this test. As shown in Fig. 4 we can see that the same increase is present. Further, the log/log curve shapes for the NE case within Figs. 3 and 4(b) are the same. We regard these observations as providing ample verification that the LM-OSL conversion technique we have used in this study leads to the same OSL shapes as could be recorded in standard CW-OSL experiments.

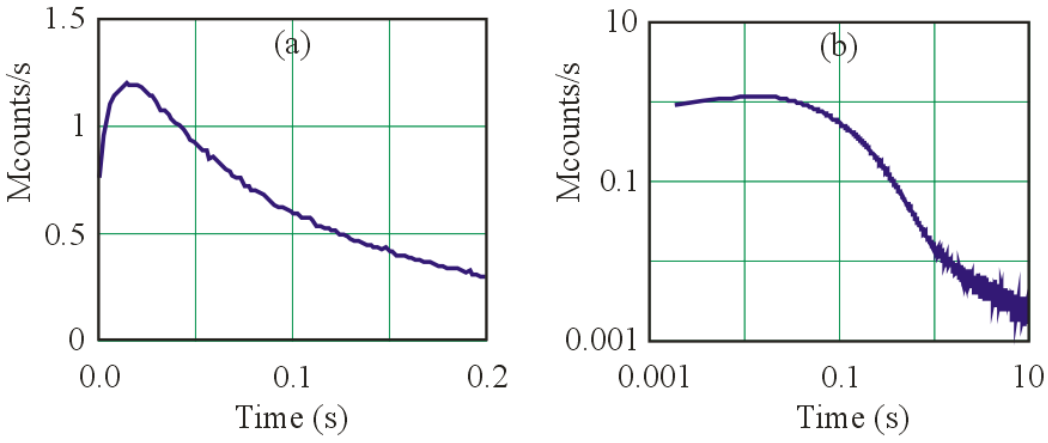

Fig. 4: CW-OSL shine example; (a) linear representation of the early shine data; (b) log/log representation of the overall shine data. The OSL was recorded at 125ºC after 9.2 Gy beta irradiation of a spent Naracoorte East (NE) aliquot; 100% blue LED stimulation applied following a 260ºC preheat; 5000 bins at 2 ms/bin resolution.

Note that the initial increase will not normally be seen when a Risø reader is set for standard dating protocols. Typical bin sizes significantly exceed those achieved at early times in the present study. We note in passing that a similar increase is apparent in synthetic quartz CW-OSL shine data presented previously by Martini and Galli (2007). [Replicated by Martini et al. (2014).] In this case, however, it appears that the increase continued for a much greater period than seen here.

The reasons underlying the existence of such increases are interesting. Indeed, they form part of our wider program. However, at the present time our investigations are incomplete. We therefore currently defer discussion on this interesting topic.

4.3.2 Luminescence steps

Clearly, the most prominent feature seen in Figs. 2 and 3 is that the luminescence appears to cascade over a number of steps when plotted in log/log form. The first step lasts for the order of a second, the second for thousands of seconds and the third for significantly longer. The steps are common to all of the quartzes we shone. We note that the first two step steps are similar to those observed within the high dynamic range time-resolved OSL study by Ankjaergaard and Jain (2010), and in OSL data presented by Wallinga et al. (2008).

The first step is both fast and intense while the second and third are progressively slower and significantly less intense. We observe that the higher intensities are offset by shorter durations, and vice versa, to the point where it can be shown simply that the areas encompassed by the successive steps are of similar magnitude. We regard this observation with some interest since it helps to guide us towards a plausible explanation for the presence of the steps. In particular, their commonality amongst all the samples we tested leads us to propose a common underlying mechanism.

4.3.3 Power law trends

Another feature of interest within the Fig. 3 luminescence data is the clear power law trend occurring towards the end of each of the steps. The relatively young high dose rate Baldina Creek (BD) sample exhibits the most prominent example. We have highlighted the trend in the case of the first step by drawing a power law asymptote, characterised by a log/log slope of -3.0. When converted into the linear domain, this line transforms into a $1/t^3$ power law decay. Although not drawn, a similar trend occurs at the end of the second step where the log/log slope is -2.0; that is, after transformation, the second step trends towards a $1/t^2$ power law decay.

The observation of power law trends in luminescent decays is not new. In particular, we refer to Huntley (2006), within which mechanisms suggested in earlier literature are discussed and an alternative electron tunnelling mechanism is suggested. None of the suggested mechanisms has, however, been confirmed.

The trends we report here certainly lie within our interest, the more so because the powers extracted above are integers. Within a separate part of our wider program we have studied the power law trend. This study, however, is reserved for future consideration.

5. Analysis

5.1 Energy band gap model

The energy band gap model for explaining luminescence in quartz is widely accepted, to the point where for many years it has become established as the standard for both modelling (Aitken, 1985; Bailey et al., 1997; Bailey, 2001) and optical dosimetry (Wintle and Murray, 2006). Within the model, it is suggested that trapped electrons are excited into the conduction band. Luminescence is emitted following subsequent radiative recombination with a hole trapped near to the valence band.

A characteristic feature of the model is that it is based on the solution of a series of rate equations, the combination of which leads to overall solutions of varying complexity depending on the variety of processes that are included. [See, for example, Bailey, 2001, Preusser et al., 2009 and many of the reference therein.] In essence, the model depends on the combination of a series of random components, each characterised by an exponential decay. The shape of OSL decay curves in quartz have therefore commonly been fitted to a linear summation of exponential curves, as discussed above in Section 1. Notably, in their exploratory work, Smith and Rhodes (1994) first fitted to three curves, commonly termed 'fast', 'medium' and 'slow'. Further slow components were later added (Bulur et al., 2000, Singarayer and Bailey, 2003, Jain et al., 2003), and an ultrafast component (Jain et al., 2008) has since been identified.

Bailey et al. (1997) showed that although the band model includes second-order retrapping, the latter will only lead to the prediction of non-exponential decays if the paths available to the released electrons change in their relative proportions during an OSL measurement. This has since been shown to be generally true for the fast, medium and slow components. We note, however, that Singarayer and Bailey (2003) observed early saturation characteristics in one of the slower components they identified. A more complex decay structure was observed by Ankjaergaard and Jain (2010). There, they also observed a step in luminescence within their time-resolved OSL measurements and described it in terms of a kinetic model comprised of four energy levels. Evidently, it is possible to construct empirical band gap models to explain many OSL decay features and, through use of multi-order processes, possibly the presence of steps.

While the band gap model can be adapted to predict non-exponential behaviour, a problem remains in relation to the physical meaning of the component processes. In any model, each component introduced for curve fitting purposes needs to be linked to a separate physical process. With regard to the present study, it is clear that a number of features within the decay curves presented here need explanation. Prominently, the steps add to the general complexity of the decay profiles, to the extent that they are difficult to explain in terms of the standard model. Further, it is quite clear that the initial increase evident in each of Figs. 3 to 5 is difficult to replicate via any combination of decay processes. At the very least, the standard model does not therefore appear to provide a simple means for explaining the present observations.

That being stated, we recognise that the model has served the luminescence field well and, indeed, still provides the basis for optical dosimetry (Wintle and Murray, 2006). It is our view, however, that the model is not particularly well-suited for explaining the present observations. Rather than extending its complexity with no clear link to quartz structural features and charge carrier dynamics, our preference here is to examine the defect pair model alternative.

5.2 Defect pair model

The defect pair model introduced by Itoh et al. (2001, 2002) is quite different in that it is based on the underlying structure of quartz and the influence of its extrinsic defects. As such the defect pair model is inherently physical in nature.

The structure of quartz has been well-described in the literature. [Refer, for example, to Preusser et al., 2009 and to the website description and visualisation by Akhavan, 2012.] In relation to the present study, the most significant geometrical aspect is the large number of empty channels lying in parallel along one axis, called c-channels. These are surrounded by dual 6-fold helices built from interlinked SiO_4 tetrahedra. It is both the c-channels and the helices that are significant to quartz luminescence. The channels are large enough for small interstitial cations such as H^+, Li^+ and Na^+ to move when freed by ionising events. Electrons and holes also move by winding along the chain of oxygen atoms within the helices. The holes can be trapped at oxygen vacancies and also by impurity atoms that substitute for Si such as Al, Ge and Ti.

We have sketched one of a multitude of possible defect distributions in Fig. 5, based loosely on an assumption that the impurity atoms are randomly spaced. We acknowledge that random spacing may not be representative of the actual distributions found in natural samples. [See, for example, Wark and Watson, 2006.] Within our present context, however, the exact nature of the distribution is of little consequence.

Within the diagram, M^+ refers either to H^+, Li^+ or Na^+, while X represents the substitutional defect responsible for storing luminescent energy. Both Ge and Ti have been suggested as candidates. Recent research by Vaccaro et al. (2017) has supported Ge but, as discussed by Williams and Spooner (2018), the identity of X still appears to be unresolved. We therefore choose to retain the generic label X.

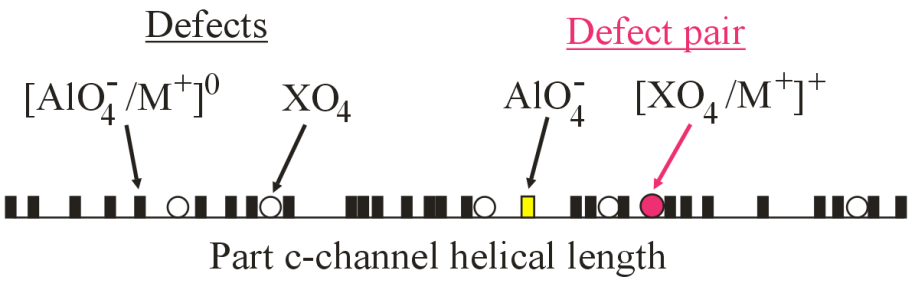

Fig. 5: Schematic defect populations along part of a c-channel helical wall, including a representative defect pair

The impurity centres that commonly exist in quartz are represented to the left of the Fig. 5 diagram, while a defect pair that can be formed during an ionising radiation process is illustrated to the right. Within their model, Itoh et al. (2002) presented a number of reactions involving defect pairs in proposing physical explanations for the well-known 110°C and 325°C quartz thermoluminescence bands, as well as quartz OSL. In a recent study, Williams and Spooner (2018) have shown that their 110°C reaction pair can also be attributed to the 160°C and 220°C thermoluminescence band emissions.

In the specific case of OSL, Itoh et al. (2002) proposed that the absorption of a stimulating photon induces the ejection of a hole from the $[XO_4/M^+]^+$ trap illustrated in Fig. 5, after which the hole can diffuse along the helix in which it was released to a position where it can be radiatively absorbed at the uncompensated AlO_4^- site (the luminescence centre), leading to the emission of 365 nm band radiance.

Although pulsed OSL measurements from within our wider program point to a more complex set of processes, the utility of the defect pair model remains intact. All we need to recognise here is that absorption of the stimulating photon leads to the emission of a charge carrier which undergoes a number of processes during its motion towards the luminescence centre. Since our analysis below does not depend on the actual identity of the carrier, we prefer at this time to use the generic terms 'charge carrier' and 'carrier' in explaining the underlying physical processes.

5.3 Defect pair occurrence in natural quartz

Before we commence our analysis it is worthwhile briefly digressing to estimate the likely occurrence of defect pairs. Impurity concentrations are well-known in the case of natural quartz, but cover a considerable range of variability. [See, for example, Göetz and Plötz , 1997, Plötz et al., 2012, and Müller *et al.*, 2012.] Typical values extracted from Plötz et al. are 166 ppm for Al, 6.6 ppm for Ti and 0.8 ppm for Ge. By utilising structural data from Akhavan (2012) together with the mass of our samples, it is not difficult to estimate the number of impurity atoms that are present. By further taking account of the collection efficiency in our system together with the total OSL counts we record, we can simply estimate the total number of OSL photons that are globally emitted from our samples into 4π steradians. We find that the latter are respectively three and four decades smaller than the numbers of Ge and Ti atoms present in our samples. The presence of defect pairs giving rise to luminescence is therefore a rarity.

5.4 Defect pair model luminescent step explanation

5.4.1 Carrier hopping

We now turn our attention to the prominent steps observed within Figs. 2 and 3. In particular, we highlight the significance of the positional locations of the two species that comprise the defect pair; that is, $[XO_4/M^+]^+$ trap and the complementary AlO_4^- luminescence centre, both sketched in Fig. 5. There, we have chosen to draw a specific case; namely, that within which the trap and luminescence centre are separated by a single XO_4 tetrahedron. The latter represents an unoccupied trap. Note that we could instead have chosen to draw the defect pair partners in such a way that no unoccupied traps intervened, or for that matter, more than one.

Let us consider the simplest case where no trap intervenes. After optical stimulation, the released carrier diffuses from the trap and is subject to an electrostatic drift force as it traverses the potential well that surrounds the trap. Diffusion and drift forces therefore govern the probability that the carrier will escape the trap. Detailed discussion of the carrier dynamics, however, lies outside of the scope of the present paper.

One feature, however, is significant within the present context; that is, a 50% probability exists that the carrier will be released towards the luminescence centre and a 50% probability that it will be released in the opposite direction. In each case, the carrier can be retrapped at its source. However,

the cases differ in a notable way. In the first case, a finite probability exists that the carrier will reach the luminescence centre while in the second case, a finite probability exists that it will reach the next furthest trap. In the first case the OSL reaction will be completed while in the second case the carrier will be trapped remotely. Following further optical stimulation the carrier can then either move back to its original trap or further away to be trapped even more remotely.

What we describe here is a hopping process. Optical stimulation events lead to the release of the charge carrier and its successive hopping amongst the traps within its locality. The location of the carrier relative to the luminescence centre therefore represents a dynamic process.

5.4.2 Luminescent steps

We are now in a position to offer a qualitative explanation for the luminescence steps seen in Figs. 2 and 3. We label the first step as the nearest neighbour (NN) case where no trap intervenes. Given favourable dynamics, the carrier generated as the outcome of any one optical stimulation event will succeed in reaching the luminescence centre, in which case OSL will be recorded. In contrast, if the circumstances are unfavourable, no luminescence will be generated and the carrier will be retrapped. Only successful transfers, therefore, lead to the generation of luminescence. In essence, we only record successful events. Furthermore, the OSL process will be expected to be relatively fast since no physical impediment exists between the trap and luminescence centre.

We label the second step the nearest-nearest neighbour (NNN) case. This case is different since an impediment to successful carrier transport is clearly present; namely, the existence of an empty trap lying between the source trap and its complementary luminescence centre. In this case, carrier hopping is important. In order to successfully reach the luminescence centre, the carrier is exposed not to a single hop in the right direction but to two hops; that is, the carrier must experience a minimum of two successful photon stimulation events before it can reach the luminescence centre. The cumulative probability of success is therefore lower, to the point where a significantly longer time is required in order to effect the emptying of all such traps. Correspondingly, the OSL intensity is significantly lower.

Clearly, the case where two empty traps intervene (labelled NNNN) is even slower and less intense. The existence of the steps observed in Figs. 2 and 3 is therefore explained. The first step (NN) is both fast and intense, the second (NNN) less fast and less intense and the third (NNNN) even more so.

In view of the clear locational nature of this model, it is interesting to ask the question as to how likely the successive traps are originally occupied in natural samples. We briefly addressed this question in Section 4.3.2 above where we noted that the area under the successive luminescence steps are of similar magnitude. This suggests the trap populations generated at the NN, NNN and NNNN sites also are similar in magnitude.

In summary, then, we consider that the Fig. 3 luminescence steps can be explained in terms of a nearest neighbour extension to the defect pair model. Indeed, we believe that such an extension provides a plausible explanation of our experimental observations. We are currently seeking further information to enable the proposed mechanism to be better verified, using a combination of LM-OSL, CW-OSL and pulsed OSL techniques.

6. Summary and conclusion

OSL has been measured from a number of South Australian natural quartz samples ranging in age from the present to around 800 ka. The measurements covered ten decades in time, during which period the OSL signal fell six to seven decades in luminescent intensity. All samples displayed a series of steps when plotted in log/log form.

In explaining the observations, both the standard energy band gap model for quartz OSL and the alternative defect pair model have been assessed. While the former could potentially be extended by increasing its complexity, we have found that the latter can be readily adapted to explain the presence of the steps via a relatively simple nearest neighbour extension. We are currently applying the defect pair model to explain a number of additional quartz OSL characteristics.

Appendix A: Data calibration procedures

A.1 LM-OSL calibration

LM-OSL operation was calibrated by replacing the U340 filter by a custom optical attenuator comprised of a stack of three thin aluminium discs interspaced by 2 mm thick commercial steel washers. A single hole was drilled in each disc, the lowest being offset by 8 mm from the centreline, the middle being centred and the top again offset by 8 mm. The attenuator provided a staggered path in allowing only a small amount of scattered light from the LED array to reach the PMT. Both 1.1 mm and 1.5 mm hole sizes were used during the calibration experiments. A blank sample disc was placed on the DA-20 carousel.

In LM-OSL mode the LEDs are driven by a ramp voltage. Examples of LM-OSL calibration measurements recorded over a range of different LED drive levels are shown in Fig. A.1. The calibration count rates are of similar scale to those recorded within the experimental runs and are considerably smaller than the levels where pulse pile-up and photocathode or preamplifier saturation effects appear. The threshold effect seen in the left panel of Fig. A.1 and the associated deviation from true linearity can therefore both be attributed to the LED drive response.

The calibration curves may be interpreted as plots of actual optical stimulation against input drive command; that is, as transfer functions. As such they are useful for offsetting both the nonlinearity and the threshold effect. Once the specific curve is selected and smoothed (in our case, the 100% curve), the maximum values on both axes can be renormalised to the 10,000 s LM-OSL run duration. With this renormalisation, the selected curve assumes transfer function form and allows actual time to be converted into a corrected time.

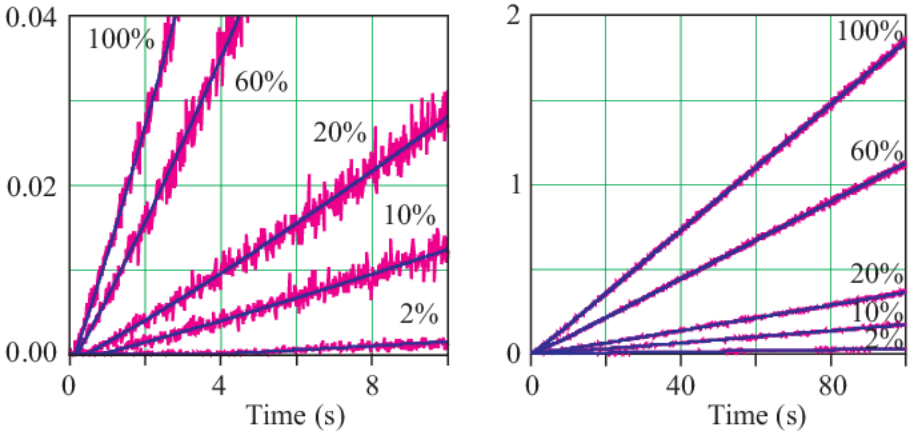

Fig. A.1: Early and late time Risø DA-20 LM-OSL calibration curves over different maximum drive levels. The vertical scales are in Mcounts/s.

As can be seen by reference to the left panel of Fig. A.1, no response occurs at early times prior to the threshold level being reached. Above threshold, the ramp rises but is characterised by a slight quadratic nonlinearity. Within our correction procedure, both these effects have been offset by replacing actual time (renormalised horizontal axis) by its corrected time equivalent (renormalised vertical axis).

A.2 Background calibration

We observed that the background increased as the optical stimulation power increased. LM-OSL was applied in order to quantify this effect, again using a blank sample disc but with the U340 filter restored into its normal position. The measured background response as the LEDs are ramped towards 100% drive is shown in Fig. A.2. It is seen that the dark current at zero drive level is ~80 counts/s and that the background rises faster than linearly as the optical power is increased. A 200 counts/s background rate is recorded at 100% drive level.

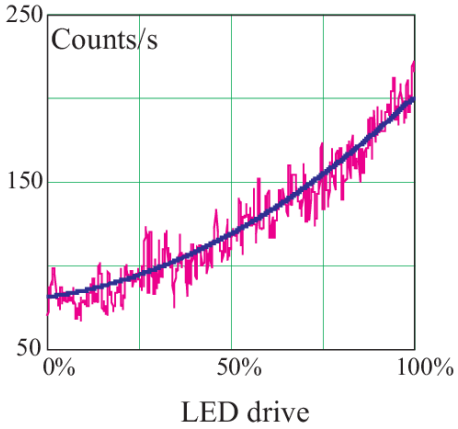

Fig. A.2: Risø DA-20 UV background response to a drive ramp towards 100% LED power.

We conducted a preliminary investigation directed towards identifying the source of the increase, during which we checked and eliminated the obvious possibility – namely, optical leakage through the U340 filter assembly. No other source was obviously apparent. We recognise, however, that

the effect may be caused by an LED wavelength change with the increasing temperature generated as the LEDs are driven to higher levels. [Refer, for example, to Jain and Lindvold, 2007.]

In view of the fact that the luminescence signal significantly exceeds the background except towards the end of each six day shine period, we have chosen at this time to defer detailed investigation. Instead, we simply subtracted the background by using the smoothed data shown in Fig. A.2.

Appendix B: Data smoothing procedure

Each of the recorded data sets was smoothed by application of a custom algorithm based on the Poisson statistical property that when a bin contains C counts the associated standard deviation is $\sqrt{C}$ counts. The smoothing problem amounts to determining how many neighbouring bins need to be amalgamated in order to achieve a targeted level of smoothness. Here, we specify the spread of counts about the local mean in terms of its extent in covering a number s of standard deviations. For the present purpose a good choice is $s = 5$ since the spread then covers much of the central part of the distribution curve.

Now, if we amalgamate N neighbouring bins each containing a mean count C, the associated spread is $s\sqrt{NC}$. Hence, if we desire to achieve a level of smoothness such that the spread does not exceed a specified fraction f of the total counts NC, then,

$$s\sqrt{NC} \le fNC \text{ , which is easily rearranged to give } N \ge \frac{s^2}{f^2 C}.$$

In practice, we chose $s = 5$ and $f = 0.03$ (3%) and applied the above relationship in order to calculate the number of bins needing to be amalgamated at each count value C. We found that no amalgamation was required at early times while at late times no more than ten bins needed to be combined. Since the late shine signal varies only slowly, no significant distortion was introduced by the smoothing procedure.

Appendix C: LM-OSL conversion to CW-OSL

Analytically, the LM-OSL signal needs to be transformed into an equivalent CW-OSL form. We note that earlier-developed transformations are generally specific to first order kinetics. [See, for example, Bulur, 2000.] In our case, we require a general transformation which is independent of knowledge the shape of the shine curve.

In developing the required transform we recognise that the significant bin parameter is not the bin period dt but the number of stimulation photons dq_{in} delivered to the sample within that period; *viz.*,

$$dq_{in} = \Phi_{in}\, dt, \qquad (1)$$

where Φ_{in} is the illuminating photon flux. Since Φ_{in} is constant in the case of CW-OSL, eqn (1) can be integrated trivially to yield the total number of photons delivered at time $t = t_{\mathrm{CWOSL}}$ as

$$q_{in} = \Phi_{in} t_{\mathrm{CWOSL}}. \tag{2}$$

In examining the luminescent response, it is convenient to introduce a response function $g(t)$ which we specify as the number of luminescence photons recorded per stimulation photon; that is, $g(t)$ is a function we introduce here to specify a general shape for the CW-OSL decay curve. The luminescent count rate is then obtained immediately by multiplying the right hand side of (1) by $g(t)$, in which case

$$\left.\frac{dq_{out}}{dt}\right|_{\mathrm{CWOSL}} = \Phi_{in}\, g(t). \tag{3}$$

In the corresponding LM-OSL case, the stimulation power ramps linearly with time. Accordingly, we find that

$$dq_{in} = \Phi(t)\, dt = \Phi_{in}\left(\frac{t}{t_{\max}}\right) dt \tag{4}$$

which integrates to

$$q_{in} = \tfrac{1}{2}\left(\frac{\Phi_{in}}{t_{\max}}\right) t^2. \tag{5}$$

By equating (2) and (5), we are immediately able to derive the relationship

$$t_{\mathrm{CWOSL}} = \tfrac{1}{2}\, t_{\max}\left(\frac{t_{\mathrm{LMOSL}}}{t_{\max}}\right)^2, \tag{6}$$

where we have defined $t = t_{\mathrm{LMOSL}}$ as the time over which LM-OSL needs to be applied in order to deliver the same number of stimulation photons as within the equivalent CW-OSL time t_{CWOSL}.

In the case of the luminescent response, the LM-OSL photon rate is derived in the same manner as eqn (3) except that Φ_{in} must be replaced by its time-dependent LM-OSL equivalent $\Phi(t)$ defined above within eqn (4). We therefore obtain

$$\left.\frac{dq_{out}}{dt}\right|_{\mathrm{LMOSL}} = \Phi_{in}\left(\frac{t}{t_{\max}}\right) g(t). \tag{7}$$

Direct comparison with the OSL equivalent result, eqn (3), yields the required luminescence count rate transformation:

$$\left.\frac{dq_{out}}{dt}\right|_{\mathrm{CWOSL}} = \Phi_{in}\, g(t) = \left(\frac{t_{\max}}{t_{\mathrm{LMOSL}}}\right)\left.\frac{dq_{out}}{dt}\right|_{\mathrm{LMOSL}}, \tag{8}$$

where again, t_{LMOSL} has been substituted for t. Together, eqns (6) and (8) enable LM-OSL time and count rate to be transformed generally into their respective CW-OSL forms.

Acknowledgments

We wish to thank the reviewers for their interest in this work and for their many suggestions. In particular, we acknowledge their input in suggesting that the increase in background illustrated in

Fig. A2 could be the result of increasing LED temperature. We further thank the reviewer who alerted us to the earlier time-resolved OSL study by Ankjaergaard and Jain (2010).

References

Aitken, M.J., 1985. *Thermoluminescence dating*. Academic Press, London.

Aitken, M.J., and Smith, B.W., 1988. Optical dating: recuperation after bleaching. Quaternary Sci. Rev. 7, 387-393.

Akhavan, A. C., "The Quartz Page: Quartz Structure," 2012, http://www.quartzpage.de/gen_struct.html

Ankjærgaard, C., and Jain, M., 2010. Optically stimulated phosphorescence in quartz over the millisecond to second time scale: insights into the role of shallow traps in delaying luminescent recombination. J. Phys. D: Appl. Phys. 43: 255502, 12pp.

Bailey, R.M., Smith, B.W., and Rhodes, E.J., 1997. Partial bleaching and the decay form characteristics of quartz OSL. Rad. Meas. 27, 123-136.

Bailey, R.M., 2001. Towards a general kinetic model for optically and thermally stimulated luminescence of quartz. Rad. Meas. 33, 17-45.

Banerjee, D., Hildebrand, A.N., Murray-Wallace, C.V., Bourman, R.P., Brooke, B.P., and Blair, M., 2003. New quartz SAR-OSL ages from the stranded beach dune sequence in south-east South Australia. Quaternary Science Reviews 22, 1019-1025.

Belperio, A.P., and Cann, J.H., 1990. Quaternary evolution of the Robe-Naracoorte coastal plain: an excursion guide. Dept of Mines and Energy, Report no. 90/27, Adelaide, South Australia.

Bøtter-Jensen, L., Bulur, E., Duller, G.A.T., and Murray, A.S., 2000. Advances in luminescence instrument systems. Rad. Meas. 32, 523-528.

Bøtter-Jensen, L., Andersen, C.E., Duller, G.A.T., and Murray, A.S., 2003. Developments in radiation, stimulation and observational facilities in luminescence measurements. Rad. Meas. 37, 535-541.

Bulur, E., 2000. A simple transformation for converting CW-OSL curves to LM-OSL curves. Rad. Meas. 32, 141-145.

Bulur, E., Bøtter-Jensen, L., and Murray, A.S., 2000. Optically stimulated luminescence from quartz measured using the linear modulation technique. Rad. Meas. 32, 407-411.

Göetz, J. and Plötze, M., 1997. Investigation of trace-element distribution in detrital quartz by Electron Paramagnetic Resonance (EPR). Eur. J. Mineral. 9, 529-537.

Grün, R., Wells, R., Eggins, S., Spooner, N.A., Aubert, M., Brown, L., and Rhodes, E., 2008. Electron spin resonance dating of South Australian megafaunal sites. Aust. J. Earth Sci. 55, 917-935.

Huntley, D.J., Hutton, J.T., and Prescott, J.R., 1993a. The stranded beach-dune sequence of south-east South Australia: a test of luminescent dating, 0-800 ka. Quaternary Science Reviews 12, 1-20.

Huntley, D.J., Hutton, J.T., and Prescott, J.R., 1993b. Optical dating using inclusions within quartz grains. Geology 21, 1087-1090.

Huntley, D.J., Hutton, J.T., and Prescott, J.R., 1994. Further luminescence dates from the dune sequence in the south-east of South Australia. Quaternary Science Reviews 13, 201-207.

Huntley, D.J., and Prescott, J.R., 2001. Improved methodology and new thermoluminescence ages for the dune sequence in south-east South Australia. Quaternary Science Reviews 20, 687-699.

Huntley, D.J., 2006. An explanation of the power-law decay of luminescence. J. Phys.: Condens. Matter 18, 1359-1365.

Itoh, N., Stoneham, D. and Stoneham, A.M., 2001. The predose effect in thermoluminescent dosimetry. J. Phys.: Condens. Matter, 13, 2201-2209.

Itoh, N., Stoneham, D. and Stoneham, A.M., 2002. Ionic and electronic processes in quartz: Mechanisms of thermoluminescence and optically stimulated luminescence. J. Appl. Phys. 92, 5036-5044.

Jain, M., Murray, A.S., and Bøtter-Jensen, L., 2003. Characterisation of blue-light stimulated luminescence components in different quartz samples: implications for dose measurement. Rad. Meas. 37, 441-449.

Jain, M., and Lindvold, L. R., 2007. Blue light stimulation and linearly modulated optically stimulated luminescence. Ancient TL, 25, 69-80.

Jain, M., Choi, J.H., and Thomas, P.J., 2008. The ultrafast OSL component in quartz: origins and implications. Rad. Meas. 43, 709-714.

Kuhns, C.K., Agersnap Larsen, N., and McKeever, S.W.S, 2000. Characteristics of LM-OSL from several different types of quartz. Rad. Meas. 32, 413-418.

Martini, M., and Galli, A., 2007. Ionic mechanisms in the optically stimulated luminescence of quartz. Phys. Stat. Sol. (c) 4, 1000-1003.

Martini, M., Fasoli, M., and Villa, I., 2014. Defect studies in quartz: Composite nature of the blue and UV emissions. Nucl. Instrum. Methods B 327, 15-21.

Moffatt, J.E., *Testing the TT-OSL single-aliquot protocol for quartz sediment dating*, 2014. M.Phil. thesis, School of Chemistry and Physics, University of Adelaide, South Australia.

Müller, A., Wanvik, J.E., and Ihlen, P.M., 2012. Petrological and chemical characterisation of high-purity quartz deposits with examples from Norway. Chap.4 in *Quartz: deposits, Mineralogy and Analytics*, Göetz, J. and Möckel, R., eds, Springer-Verlag, Heidelberg.

Oniya, E.O., Polymeris, G.S., Tsirliganis, N.C., and Kitis, G., 2012. On the pre-dose sensitisation of the various components of the LM-OSL signal of annealed quartz; comparison with the case of the 110C TL peak. Rad. Meas. 47, 864-869.

Plötze, M., Wolf, D., and Krbetschek M.R., 2012. Chap. 8, Gamma-irradiation dependency of EPR and TL spectra of quartz, within Göetz, J. and Möckel, R., eds, *Quartz: deposits, Mineralogy and Analytics*, Springer-Verlag, Heidelberg.

Preusser, F., Chithambo, M.L., Götte, T., Mancini, M., Ramseyer, K., Sendezera, E.J., Susino, G.J., and Wintle, A.G., 2009. Quartz as a natural luminescence dosimeter. Earth-Science Reviews 97, 184-214.

Risø, 2013. Guide to the Risø TL/OSL reader, Model DA-20. Risø National Laboratory for Sustainable Energy, Danish Technical University, Denmark.

Schwebel, D.A., 1983. Quaternary dune systems. In Tyler, M.J., Twidale, C.R., Ling, J.K., and Holmes, J.W. (eds), *Natural History of the South-East*, pp. 15-24, Royal Society of South Australia, Inc., Adelaide.

Singarayer, J.S., and Bailey, R.M., 2003. Further investigations of the quartz optically stimulated luminescence components: using linear modulation. Rad. Meas. 37, 451-458.

Smith, B.W., Aitken, M.J., Rhodes, E.J., Robinson, P.D., and Geldard, D.M., 1986. Optical dating: methodological aspects. Radiation Protection Dosimetry 17, 229-233.

Smith, B.W., and Rhodes, E.W., 1994. Charge movements in quartz and their relevance to optical dating. Rad. Meas. 23, 329-333.

Vaccaro, G., Panzeri, L., Paleari, S., Martini, M., and Fasoli, M., 2017. EPR investigation of the role of germanium centres in the production of the 110ºC thermoluminescence peak in quartz. Quaternary Geochronology **39**, 99-104.

Wallinga, J., Bos, A.J.J., and Duller, G.A.T., 2008, "On the separation of quartz OSL signal components using different stimulation modes," Rad. Meas. 43, 742-747.

Wark, D.A., and Watson, E.B., 2006. TitaniQ: a titanium-in-quartz geothermometer. Contrib. Mineral Petrol. 152, 743-754.

Williams, O.M., and Spooner, N.A., 2018, "Defect pair mechanism for quartz intermediate temperature thermoluminescence bands," Rad. Meas. 108, 41-44.

Wintle, A.G., and Murray, A.S., 2006. A review of quartz optically stimulated luminescence characteristics and their relevance in single-aliquot regeneration dating protocols. Rad. Meas. 41, 369-391.